Dzyaloshinskii-Moriya anisotropy and nonmagnetic impurities in the $s=\frac{1}{2}$ kagome system $ZnCu_3(OH)_6Cl_2$

Ioannis Rousochatzakis,[1] Salvatore R. Manmana,[1] Andreas M. Läuchli,[2] Bruce Normand,[1] and Frédéric Mila[1]
[1]*Institute of Theoretical Physics (CTMC), École Polytechnique Fédérale de Lausanne, CH-1015 Lausanne, Switzerland*
[2]*Max-Planck-Institut für Physik komplexer Systeme, D-01187 Dresden, Germany*
(Received 16 March 2009; revised manuscript received 12 May 2009; published 11 June 2009)

Motivated by recent nuclear magnetic resonance experiments on $ZnCu_3(OH)_6Cl_2$, we present an exact-diagonalization study of the combined effects of nonmagnetic impurities and Dzyaloshinskii-Moriya (DM) interactions in the $s=1/2$ kagome antiferromagnet. The local response to an applied field and correlation-matrix data reveal that the dimer freezing which occurs around each impurity for $D=0$ persists at least up to $D/J\simeq 0.06$, where J and D denote, respectively, the exchange and DM interaction energies. The phase transition to the $(Q=0)$ semiclassical 120° state favored at large D takes place at $D/J\simeq 0.1$. However, the dimers next to the impurity sites remain strong up to values $D\sim J$, far above this critical point, and thus do not participate fully in the ordered state. We discuss the implications of our results for experiments on $ZnCu_3(OH)_6Cl_2$.

DOI: 10.1103/PhysRevB.79.214415 PACS number(s): 75.10.Jm, 75.30.Gw, 75.30.Kz, 75.40.Cx

I. INTRODUCTION

The $s=1/2$ antiferromagnetic (AFM) Heisenberg model on the two-dimensional kagome lattice is one of the simplest models in frustrated quantum magnetism, but displays some of the most complex behavior known.[1] As such, it has for decades maintained its position at the forefront in the search for novel quantum-mechanical phases of matter, such as the resonating-valence-bond (RVB) spin-liquid state proposed initially by Anderson.[2] The nature of the ground state of the $s=1/2$ kagome AFM has still not been fully established: the variety of competing phases proposed in the literature includes valence-bond crystals (VBCs),[3] gapped spin liquids,[4–6] and gapless critical phases.[7,8] Under these circumstances, the discovery that the kagome AFM is extremely sensitive even to the smallest perturbations, such as the presence of anisotropies[9,10] or of nonmagnetic impurities,[11,12] is completely consistent.

In this context, the recent discovery[13] of the mineral herbertsmithite, $ZnCu_3(OH)_6Cl_2$, has attracted very considerable attention because it represents a structurally perfect realization of the $s=1/2$ kagome AFM. This material is composed of Cu^{2+} ions $(s=1/2)$ arranged on kagome planes separated by triangular layers of nonmagnetic Zn^{2+} ions. Despite the large AFM exchange, $J\simeq 170-190$ K in this material,[14,15] in experiment there is no evidence of long-ranged magnetic order or even of spin freezing at any temperatures down to 50 mK.[16,17] There is in addition no sign of a spin gap in the excitation spectrum.[17,18]

However, it has also been established that in $ZnCu_3(OH)_6Cl_2$ there is a significant (5%–10%) intersite exchange of Cu^{2+} ions with the Zn^{2+} ions intended to separate the kagome planes.[19,20] The displaced Cu^{2+} ions are thought to account for the large Curie tails observed in powder susceptibility measurements[17,21] and for the field-dependent Schottky-like anomaly in the specific heat.[20] At the same time, the Zn^{2+} ions displaced into the kagome planes play the role of nonmagnetic vacancies, which are known[11,12] to modify the ground-state properties in a nontrivial way. However, these impurities can also be considered as a probe of kagome physics, and in this respect the recent ^{17}O nuclear magnetic resonance (NMR) experiments reported by Olariu *et al.*[18] offer extensive insight. While each O^{2-} ion is coupled predominantly to two neighboring Cu^{2+} ions in the kagome planes, the NMR spectra revealed a broad distribution of local susceptibilities. The relative 1:2 ratio between the line shifts of the two leading features in the ^{17}O spectrum was explained on the basis of distinguishing between two groups of O sites in the doped kagome planes, those ["Defect" (D)] probing the magnetic polarization directly next to an impurity site, and hence coupled only to one Cu spin, and those ["Main" (M)] reflecting the polarizations of all other sites. This interpretation was also consistent with the relative intensities of the two lines based on the expected in-plane dopant concentration of approximately 5%. Another major finding of these experiments was the observation that the M and D line shifts approach a finite value as $T\to 0$, suggesting a nonsinglet ground state without a gap. This result can also be inferred from the nonactivated behavior of the nuclear spin-lattice relaxation rate, $1/T_1$, at low temperatures.[18]

While the true nature of the nonmagnetic ground state of the pure, $s=1/2$ Heisenberg kagome AFM remains unknown, all of the guidance obtained from VBC or RVB constructions suggests a total singlet. Indeed, the nearest-neighbor RVB basis has been shown to deliver a semiquantitative account of some of the properties of the system, both without[5,22] and with[11] impurities, and for this reason a nonsinglet ground state presents a considerable challenge. However, by the nature of its structure, a triangular geometry involving active $d_{x^2-y^2}$ and $d_{3z^2-r^2}$ orbitals, the Cu–Cu bonds in $ZnCu_3(OH)_6Cl_2$ are not centrosymmetric. The resulting Dzyaloshinskii-Moriya (DM) interactions[23] induce quite generally a small admixture of triplet states into a singlet ground state,[14] and thus have been discussed[18] as a likely explanation for the finite response observed at zero temperature. The DM interactions in herbertsmithite have been determined recently by electron spin resonance experiments.[24] These measurements show that the dominant

component of the DM interaction is that perpendicular to the kagome plane, which is of order $D \simeq 15$ K $\sim 0.08J$, while the in-plane component, D', although not excluded by symmetry, is much smaller ($D' \simeq 2$ K $\sim 0.01J$).

Clearly, a complete theoretical description for the ground-state properties of $ZnCu_3(OH)_6Cl_2$, including the magnetization response around the impurity sites, must take into account the combined effect of both the DM interactions and the nonmagnetic impurities in the kagome planes. Among the many approaches adopted to gain further insight into the kagome system, it is well known that the clean classical kagome AFM without DM anisotropy has an extensive ground-state degeneracy,[25] which is fully lifted by quantum fluctuations only beyond harmonic order.[26–28] The inclusion of DM anisotropy perpendicular to the kagome plane selects immediately the uniform ($Q=0$) three-sublattice state.[9,10] Cépas *et al.* showed recently[29] that in the quantum ($s=1/2$) kagome AFM, this ordered phase can be stabilized only for $D/J \gtrsim 0.1$. This implies that herbertsmithite may well be very close to the critical point where quantum fluctuation effects promote a disordered ground state. The linear susceptibility of the clean kagome AFM in the presence of DM interactions has been analyzed[30] using a perturbative expansion about a short-ranged VBC ground-state scenario, while the effect of nonmagnetic impurities without DM interactions has been studied in Refs. 11, 12, 31, and 32. It has been shown that one of the central consequences of a nonmagnetic impurity in the quantum kagome AFM is a characteristic dimer freezing, which takes place around the impurity site due to frustration relief in the affected triangles.[11,12]

Here we present an extensive exact-diagonalization study which includes the effects of both DM anisotropy and nonmagnetic impurities. Our results can be summarized as follows. For $D/J \lesssim 0.06$, the effect of frustration relief around the impurity[11,12] causes the formation of strong local dimers whose magnetization response, a staggered moment directed along $\mathbf{D}\times\mathbf{B}$, is qualitatively similar to that of isolated dimers. In this regime we find surprisingly large variations in the magnitude of the response on the different induced dimers. For sites far away from the impurity, we argue that the response must be uniform and much smaller in magnitude. For $D/J \gtrsim 0.1$, the system enters the $Q=0,120°$ semiclassically ordered state,[9,10,29] and the effect of impurities becomes very short-ranged. However, even here we find that the dimers next to the impurity remain strong up to values $D/J \sim 1$, meaning that their spins remain correlated with each other, rather than participating in the ordered state, for $D/J \lesssim 1$.

This article is organized as follows. In Sec. II we introduce the model Hamiltonian and discuss some of the symmetry aspects of the clusters considered in our exact-diagonalization calculations. The results for the local magnetization response are presented and analyzed in Sec. III. In Sec. IV, we investigate the dominant magnetic correlations on the basis of the full correlation matrix (the "natural orbital" method). We conclude in Sec. V with a discussion of the implications of our results for experimental measurements on $ZnCu_3(OH)_6Cl_2$. We also include two appendices which elaborate on the magnetization response of a minimal (four-site) cluster (Appendix A) and on the natural orbital method (Appendix B).

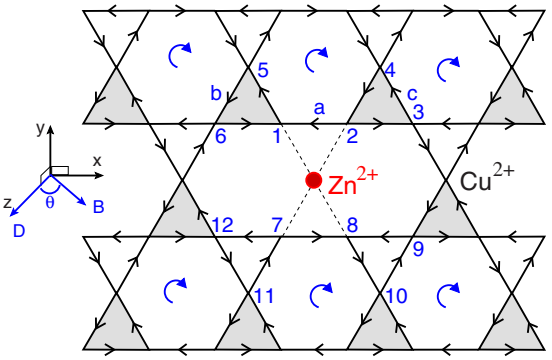

FIG. 1. (Color online) The kagome lattice of Cu^{2+} ions ($s=1/2$), containing a single nonmagnetic Zn^{2+} impurity. Bond arrows define site labels i and j in each interaction term $\mathbf{D}\cdot\mathbf{s}_i\times\mathbf{s}_j$, while $\mathbf{D}=D\mathbf{e}_z$ with $D>0$ for all bonds. Curving arrows denote the $\mathbf{C}_6$ symmetry about the hexagon centers.

II. MODEL

We consider a spin-1/2 model on the kagome lattice with a single nonmagnetic impurity described by the Hamiltonian

$$\mathcal{H} = J\sum_{\langle ij\rangle} \mathbf{s}_i\cdot\mathbf{s}_j + \sum_{\langle ij\rangle} \mathbf{D}_{ij}\cdot(\mathbf{s}_i\times\mathbf{s}_j) - \mathbf{B}\cdot\mathbf{S}, \qquad (1)$$

with periodic boundary conditions. The first term is the Heisenberg exchange energy between nearest-neighbor spins $\langle ij\rangle$, the second term represents the DM interactions, and the last term is the Zeeman energy of the total spin $\mathbf{S}=\Sigma_i\mathbf{s}_i$ in a field $\mathbf{B}$. In what follows, we work in the fixed reference frame xyz shown in Fig. 1. The field is taken to be in the xz plane at an angle θ from the z axis. The DM vectors on every bond are taken to be perpendicular to the kagome plane and are fixed by the symmetry of the clean system, namely, translations and $\mathbf{C}_6$ rotations around the hexagon centers. We have chosen the site-labeling convention, denoted in Fig. 1 by the directionality of the arrows from i to j, such that $\mathbf{D}_{ij}=D\mathbf{e}_z$ with $D>0$ for all bonds.

In this study we do not consider an in-plane component, D', of the DM vector. Quite generally, the in-plane DM problem on the kagome lattice is rather different from its out-of-plane counterpart, which we study here. At the classical level,[9] the presence of D' promotes a noncoplanar spin state with net ferromagnetic order, whose uniform out-of-plane magnetization component is controlled by the ratio $|D'|/J$, and a 120° structure of the xy-plane components with $\mathbf{Q}=0$. In contrast to the out-of-plane case, here the directions of the spins in the xy plane are completely fixed by the in-plane DM terms, which break explicitly all global spin symmetries. However, as noted above, in $ZnCu_3(OH)_6Cl_2$ the in-plane component of the DM vector has been found[24] to be much weaker than the out-of-plane component ($|D'/D| \sim 1/8$). Because, in addition, the in-plane component may be transformed away up to order D'^2/J by appropriate spin rotations,[29,33] this term appears rather unlikely to be relevant in determining the physics of herbertsmithite.

We will focus on the magnetization response of the system in finite fields, up to the values $B \sim 10$ T($B \lesssim J/20$) probed by experiment. For a general field orientation θ, the

U(1) spin rotation symmetry around the z axis is broken and thus the total magnetization S^z is not a good quantum number. Because of the impurity site, the same is true also for the momentum. Thus we can treat kagome clusters with a maximum of $N=26$ magnetic sites, and here we show primarily the results for $N=14$, 20, and 26. These clusters are symmetric with respect to spatial inversion through the impurity site. For a nondegenerate ground state, this sets the constraints

$$\langle \mathbf{s}_1 \rangle = \langle \mathbf{s}_8 \rangle, \quad \langle \mathbf{s}_2 \rangle = \langle \mathbf{s}_7 \rangle, \quad \langle \mathbf{s}_3 \rangle = \langle \mathbf{s}_{12} \rangle, \ldots . \tag{2}$$

Furthermore, the clusters with $N=14$ and 26 are also spatially symmetric under reflection through the xz plane which passes through the impurity site (Fig. 1), whence their Hamiltonian [Eq. (1)] remains invariant under the corresponding mirror operation (spatial reflection followed by the time reversal). For a nondegenerate ground state, this gives in addition

$$\langle s_1^{x,z} \rangle = \langle s_7^{x,z} \rangle, \quad \langle s_1^{y} \rangle = -\langle s_7^{y} \rangle,$$

$$\langle s_2^{x,z} \rangle = \langle s_8^{x,z} \rangle, \quad \langle s_2^{y} \rangle = -\langle s_8^{y} \rangle, \ldots . \tag{3}$$

This mirror symmetry is also present in the clean infinite kagome lattice. Thus if the vacant site were occupied by a spin $\mathbf{s}_0$, Eq. (3) would require $\langle s_0^y \rangle = 0$. The remaining symmetries of the clean kagome lattice would then enforce $\langle s_i^y \rangle = 0$ for all sites i, an argument we will employ below to demonstrate that in the disordered phase ($D/J \lesssim 0.1$) there can be no staggered magnetic response along the y axis sufficiently far from a vacant site.

In addition to these "symmetric" clusters, we have also investigated clusters with odd numbers of magnetic sites, particularly with $N=17$ and 23, whose ground state has a finite moment $S_z = 1/2$. As shown in Ref. 34, this moment does not form a bound state around the impurity site, as is the case in systems such as the checkerboard lattice,[34] but is delocalized over the entire cluster. Thus we expect no difference between clusters with even or odd numbers N of magnetic sites in the thermodynamic limit, and our results indeed conform with this picture.

III. LOCAL RESPONSE

Figure 2 shows the local in-plane magnetizations $\langle s_i^{x,y} \rangle$ (red arrows) and the local spin correlation functions $\langle \mathbf{s}_i \cdot \mathbf{s}_j \rangle$ (described quantitatively by the thickness of each bond ij) for the 26-site cluster with $B=J/20$ and $\theta=30°$, and for four representative values of D/J. The full D/J dependence of the in-plane magnetizations, the correlation amplitudes, and the local twist amplitudes $\langle (\mathbf{s}_i \times \mathbf{s}_j)^z \rangle$ is shown for each type of site or bond in Fig. 3. These results demonstrate that there exist two primary regimes with qualitatively different magnetic response, whose properties we discuss in detail in the following subsections. In summary, these are (i) the small-D/J regime ($D/J \lesssim 0.06$), where there is a local dimerlike response for the sites around the impurity, and (ii) the large-D/J regime ($D/J \gtrsim 0.1$), which is characterized by the expected[9,10,29] in-plane 120° magnetic ordering pattern, albeit with a special response from the sites right next to the vacancy. We also find an apparent intermediate regime ($0.06 \lesssim D/J \lesssim 0.1$) with a peculiar magnetization pattern around the impurity, but with no evidence of long-ranged magnetic correlations, and we will also characterize this to the extent that our calculations allow.

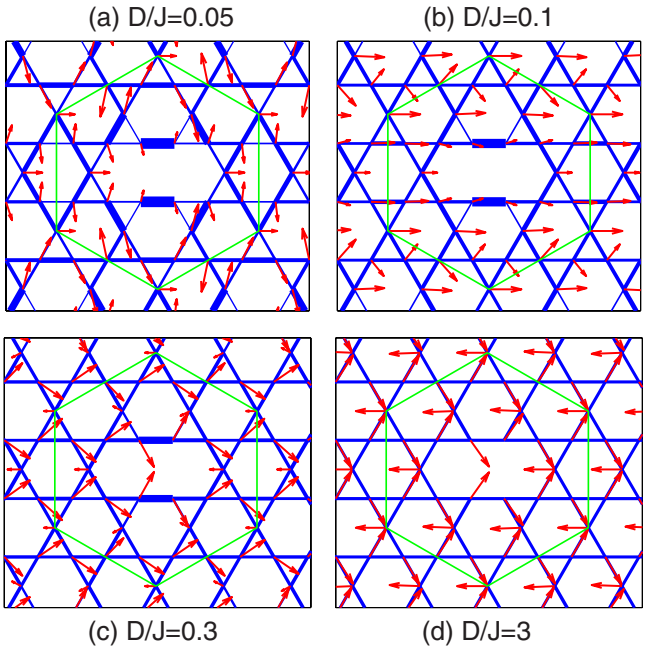

FIG. 2. (Color online) In-plane magnetizations and bond spin correlation functions for the 26-site kagome cluster with $B=J/20$ and $\theta=30°$. The lengths of the arrows are proportional to $(\langle s_i^x \rangle^2 + \langle s_i^y \rangle^2)^{1/2}$ and the thicknesses of the bonds to $\langle \mathbf{s}_i \cdot \mathbf{s}_j \rangle$.

A. $D \lesssim 0.06J$: local dimerlike response

We begin by considering the behavior of the nearest-neighbor spin correlations, $\langle \mathbf{s}_i \cdot \mathbf{s}_j \rangle$, which are shown in Fig. 3(c) and are also denoted by the bond thicknesses in Fig. 2. A low-D regime, where the correlations are controlled by the exchange interaction (J) and by the presence of the impurity,

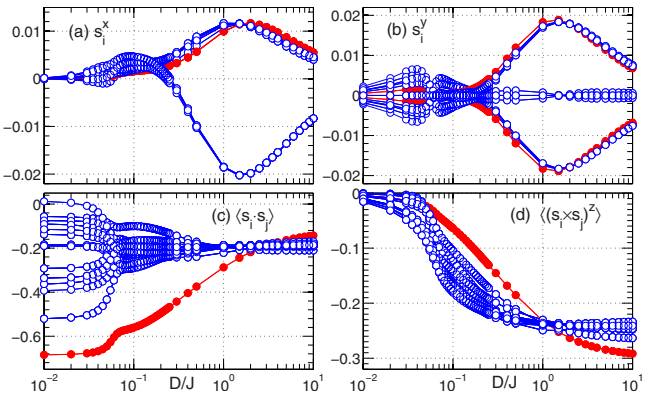

FIG. 3. (Color online) D dependence of (a) $\langle s_i^x \rangle$, (b) $\langle s_i^y \rangle$, (c) $\langle \mathbf{s}_i \cdot \mathbf{s}_j \rangle$, and (d) $\langle \mathbf{s}_i \times \mathbf{s}_j \rangle^z$ for the 26-site kagome cluster with $B=J/20$ and $\theta=30°$. i and j in panels (c) and (d) are nearest-neighbor sites only. The curves which correspond to the sites or bonds closest to the impurity are designated by (red) filled symbols.

can be seen to exist for $D/J \lesssim 0.06$, although in fact the correlation amplitudes begin to deviate from their zero-D limit at $D/J \sim 0.03$. This limit was studied in detail in Ref. 11 and is characterized by a large and oscillatory variation in the correlation amplitudes as a function of distance from the impurity. As shown in Fig. 2(a), the strongest dimerization is found on the bonds nearest the vacancy, where $\langle \mathbf{s}_i \cdot \mathbf{s}_j \rangle \simeq -0.69$ is very close to the value of -0.75 expected for an isolated dimer. This local "dimer freezing" is a key consequence of the frustration relief in the two triangles containing the vacancy[11,12] and, as we will discuss below, has direct implications for the magnetization response of the corresponding sites in the small-D/J regime.

The local twist amplitudes $\langle (\mathbf{s}_i \times \mathbf{s}_j)^z \rangle$ shown in Fig. 3(d) represent, from Eq. (1), the DM contribution to the total magnetic energy. As expected for the small D/J regime, these scale linearly with D/J for all bonds, although with a quite inhomogeneous distribution of slopes depending on the distance of the bond from the impurity. In particular, the bonds closest to the impurity have one of the smallest twist amplitudes, as might be anticipated from their strong dimerization.

Turning next to the magnetization response shown in Figs. 2(a), 3(a), and 3(b), this develops predominantly in the xy plane, as expected given the easy-plane character of the DM anisotropy, and the induced spin components are of order $\langle s_i^{x,y} \rangle \sim 10^{-3} - 10^{-2}$. By contrast, the out-of-plane response is very small ($\langle s_i^z \rangle \lesssim 10^{-6}$), and thus will not be considered in the following. With the exception of sites strongly influenced by the periodic boundary conditions, the magnetization response shows a number of features which are also present in the 20-site cluster and can be understood qualitatively on the basis of the strong local dimer formation around the impurity. Indeed, the direction of the induced magnetizations at the strongly dimerized bonds is qualitatively similar to the response expected[35] if they were isolated: a staggered polarization in the direction $\mathbf{D} \times \mathbf{B}$ (here the y axis) and a uniform polarization in the direction $(\mathbf{D} \times \mathbf{B}) \times \mathbf{D}$ (x axis). At the quantitative level, the actual magnitude of the magnetization response goes beyond the isolated-dimer picture, showing the striking feature that the moments induced on the four "next-most-strongly" dimerized bonds [bond (3,4) and its equivalents in Fig. 1] are larger by a factor of 3–4 than on the bonds closest to the impurity. The origin of this result, which we probe in detail below, is rather deeper than a simple anticorrelation between spin correlation amplitude and induced moment. It lies in the fact that, while the ground-state wave function close to the impurity can be described as an approximate product state of local dimers, the actual nature of the excitations may nevertheless differ significantly from such a picture.

To clarify this point, we isolate the sites 1–6 of Fig. 1 and consider their response in the small-D/J regime. Figure 4 shows the exact correlations and induced magnetization of this cluster with parameters $B=J/20$ and $\theta=30°$, and for the same four representative values of D/J shown in Fig. 2. Note that the magnetic response at bonds (3,4) and (5,6) is not symmetrical because the reflection symmetry relating these is broken explicitly in the presence of DM interactions. The response for $D=0.05J$ is very similar to that of the sites 1–6 in Fig. 2, and in fact the same physics can also be shown to dominate the response of a four-site cluster (sites 1–4 of Fig. 1), as detailed in Appendix A. In all cases, the magnetizations induced on bond (3,4) are larger than those on bond (1,2) by a fixed factor of up to 5. The qualitative interpretation (Appendix A) of this result lies in the different character of the local excitations on bonds (1,2) and (3,4): a triplet excitation on bond (1,2) is a true eigenstate of the isotropic Hamiltonian, whereas a similar triplet excited on the bond (3,4) is not, and may propagate away. As a result, the magnetization response of bond (1,2) is to first order in D/J the same as that of an isolated dimer, while that of bond (3,4) will be almost five times larger in the extreme case of the four-site cluster. The same arguments apply not only on the six-site cluster, but also to the impure kagome lattice, although in this latter case a triplet excitation on the bonds next to the impurity does not remain fully localized because the bonds are not fully "frozen." More generally, the qualitative agreement between the response of the smallest clusters and the response of the corresponding sites in the 20- and 26-site calculations shows that in the regime of small D/J, the magnetization profile around the impurity is governed almost entirely by local correlations.

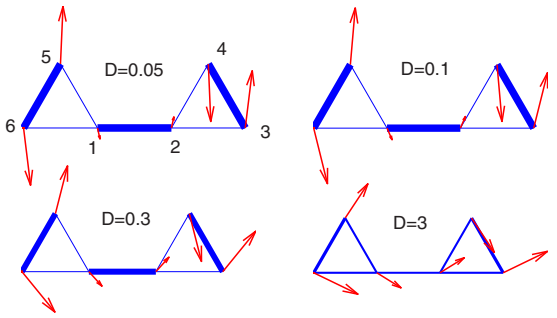

FIG. 4. (Color online) In-plane magnetization pattern (red arrows) and bond strengths (bond thickness in blue) on the isolated six-site cluster discussed in Sec. III, for $B=J/20$ and $\theta=30°$.

The magnetization response far from the impurity is expected to be that of the clean kagome lattice with DM interactions. As explained above, the staggered magnetization must vanish by symmetry, while a uniform component (along the x axis) can survive. This latter scales as $\mathbf{D} \times (\mathbf{D} \times \mathbf{B})$ (see also Ref. 30) and thus is very much weaker than the staggered response in close proximity to the impurity. This result is corroborated by exact-diagonalization calculations on a clean 12-site kagome cluster (not shown here), which reveal a very weak uniform response ($\langle s_i^x \rangle \sim 10^{-7}$). We comment that results for larger clean clusters ($N=18$ and 24) suffer from severe finite-size effects due to the presence of inequivalent loops in these geometries, and thus cannot be used for a quantitative determination of the magnetization response far from the impurity in the thermodynamic limit.

B. $D \gtrsim 0.1J$: semiclassical $Q=0,120°$ ordered state

At large values of D/J [Fig. 2(d)], the magnetization profiles correspond closely to the expected[9,10,29] $Q=0$ semiclassical three-sublattice (120°) state. We note here that in this

case the magnetic field and the impurity combine to pin one of the (infinitely many) degenerate semiclassical states. This can be understood physically from the fact that the selected configuration is the one in which the spin missing at the impurity site would be antiparallel to the field, and thus would contribute a positive Zeeman energy. However, Fig. 2(d) also shows that the spins closest to the impurity are slightly tilted away from a perfect 120° orientation. In fact these spins do not participate in the ordered state in the same way as all the other ("bulk") spins do, as can be inferred from the spin correlation amplitudes in Fig. 3(c). Above $D/J \sim 0.06$, and especially beyond $D/J \sim 0.6$, all the bonds except the two closest to the impurity attain very similar strengths. By contrast, the dimers next to the impurity (denoted by filled symbols) resist this tendency, their spins remaining strongly correlated up to surprisingly high values in excess of $D \sim J$. There is no such feature on the neighboring bonds, i.e., there is no indication of a length scale in this behavior. This is another primary consequence of frustration relief on the triangles hosting the impurity, and will be further corroborated by our analysis of the in-plane correlation data in Sec. IV.

One further comment regarding the behavior of the twist amplitude at large D/J is in order here. In the clean kagome system, the twist amplitude is the same on every bond, but according to Fig. 3(d), the sites next to the impurity have a twist amplitude, $\langle(\mathbf{s}\times\mathbf{s}_j)^z\rangle \simeq -0.3$ for $D/J \to \infty$, larger than on any of the other bonds. This reflects the fact that the relative orientation of these two spin pairs lies between the 120° orientation of the spins on triangles and the 90° orientation favored in an isolated dimer, and as such shows the consequence of frustration relief for the DM interaction.

C. Intermediate regime: $0.06 \lesssim D/J \lesssim 0.1$

Our results for the local magnetic properties (Figs. 2 and 3) imply the presence of an intermediate regime, $0.06 \lesssim D/J \lesssim 0.1$, which cannot be classed as being in either of the above limits. Here the spins develop a peculiar magnetization pattern around the impurity site, seemingly indicative of spins with no effective interaction which only follow the applied field. This is shown for the case $D/J=0.1$ in Fig. 2(c), but the analogous picture for $D/J=0.07$ is practically indistinguishable. We have investigated this regime in considerable detail as a function of D/J, of the applied field B/J, and of the field angle θ, finding essentially perfect linear response to the field down to the lowest energy scales. As we will show in Sec. IV, the in-plane magnetic correlation data show no evidence for long-ranged magnetic order in this regime.

While we cannot exclude the possibility of some type of exotic order in this regime, such as a chiral or a spin-nematic phase, we are unable to find any evidence of a local order parameter. Thus we feel that, pending further studies by other approaches, the most likely explanation for the peculiar magnetization patterns we observe lies in finite-size effects. One of the reasons that these effects are strong here is the fact that a uniform magnetic field is not the appropriate conjugate field for the three-sublattice ordered state, and thus competes with this type of order close to the critical point where the size of the ordered moment is small.

IV. MAGNETIC CORRELATIONS

Although the analysis of the local magnetization data in Sec. III reveals several major qualitative features of the ground state of Eq. (1), a number of issues remain unresolved. One is whether there exists any type of magnetic order in the window $0.06 \lesssim D/J \lesssim 0.1$, and what is the actual critical value of D/J where the 120° phase is established. Another concerns the fact that the magnetization patterns shown in Fig. 2 give few indications regarding the consequences of finite-size effects in our calculations, which may be quite different in different parameter regimes, and a method is required by which to make this more systematic. Further, the actual magnitudes of the moments in the ordered phase cannot be inferred from the local magnetization data because the latter do not represent the thermodynamic limit. While we will obtain these moments, here we will not pursue the observation, from our numerical data for the field dependence of the magnetizations at large D ($D/J \gtrsim 1$), that a very large field ($B/J \sim 1$) is required to establish their full lengths.[36]

It is thus necessary to analyze the magnetic correlations in the ground state $|\Psi\rangle$ of Eq. (1) as a function of D/J. The easy-plane character of the DM anisotropy allows us to focus on in-plane correlations, but the breaking of translational invariance by the impurity makes it necessary to consider the full set of these, which is contained in an $N\times N$ matrix with entries

$$C_{ij} = \langle\Psi|s_i^+ s_j^-|\Psi\rangle. \tag{4}$$

We remark here that an analysis based on the connected (or cumulant) correlation matrix instead of on $\mathbf{C}$ [Eq. (4)] gives the same results because for the fields considered in this study, the local magnetic moments $\langle s_i^{\pm}\rangle$ are negligibly small compared to the connected portion of the correlations, a result which is true for both small and large values of D/J. A further consequence of this is that our low-field correlation data ($B=J/20$ in the calculations to follow) are essentially identical to the $B=0$ case.

For translationally invariant systems, the correlation matrix can be partially or fully diagonalized by a simple Fourier transformation. In the present case, where translational invariance is absent due to the nonmagnetic impurity, $\mathbf{C}$ must be diagonalized numerically. The information contained in $\mathbf{C}$ is very useful, especially if the ground state contains long-ranged magnetic correlations in the xy plane. In this case, it is known (Refs. 37 and 38 and Appendix B) that the maximum eigenvalue λ_m of $\mathbf{C}$ is macroscopically large, i.e., $\lambda_m \propto N$. The corresponding eigenvector, $\boldsymbol{v}_m$, then describes the magnetic mode of the system with the dominant fluctuations, and thus is related directly to the spatial dependence of the relevant order parameter. In the case at hand, the dominant mode $\boldsymbol{v}_m$ is not simply a periodic modulation of the spins, but will contain valuable information for the nontrivial magnetization profile around the impurity. In what follows we exploit this information.

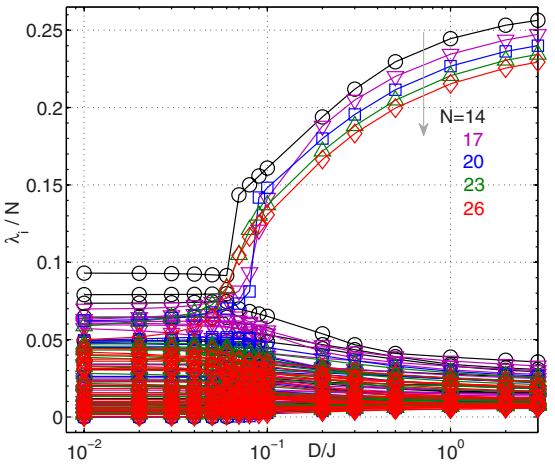

FIG. 5. (Color online) Eigenvalues λ_i of the correlation matrix (divided by N) as a function of D/J for $N=14$ (circles), 17 (down triangles), 20 (squares), 23 (up triangles), and 26 (diamonds). Here $B=J/20$ and $\theta=30°$, but the results for $B=0$ are identical.

Figure 5 shows the full eigenvalue spectrum of $\mathbf{C}$ for clusters with $N=14$, 17, 20, 23, and 26. The results for $B=0$ and $B=J/20$ are indistinguishable. An essential feature of Fig. 5 is that, as D/J is increased in the region beyond 0.06, the maximum eigenvalue on each of the clusters becomes proportional to N, and thus very much larger than the remaining eigenvalues; we caution that the actual value of this crossover cannot be inferred from the data of Fig. 5, where it is evident that the curves are still some way from the thermodynamic limit, and address this point below. As described in Appendix B, this means that the system has developed long-ranged in-plane magnetic correlations in the regime of large D/J. For small D/J, all the eigenvalues depend only weakly on D/J and are closely spaced in magnitude, which is a sign of short-range correlations dictated not by D but by J.

The finite-size scaling of the dominant eigenvalue λ_m, normalized by N, is given in Fig. 6. The extrapolated values of this quantity represent the square of the average magnetic

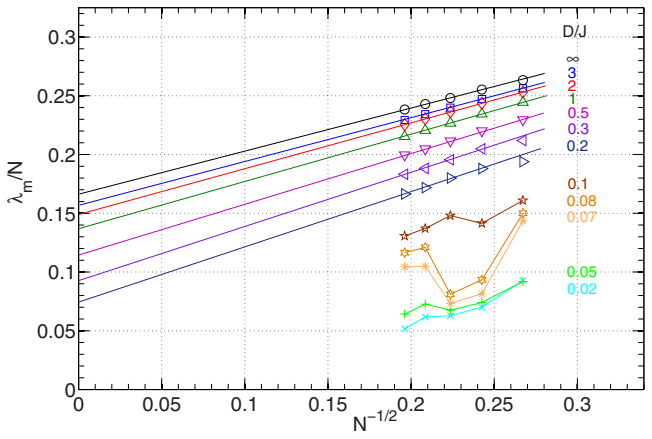

FIG. 6. (Color online) Scaling with system size of the largest eigenvalue λ_m (divided by N) of the correlation matrix. The solid lines correspond to the expected $1/\sqrt{N}$ scaling of the leading corrections to the thermodynamic limit in the 120° ordered phase.

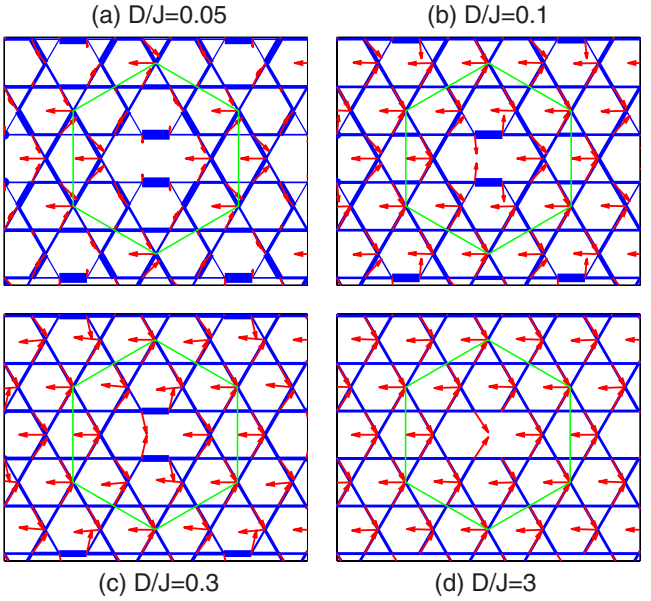

FIG. 7. (Color online) Magnetization profile for the 26-site kagome cluster in zero field, corresponding to the eigenvector $\boldsymbol{v}_m$ of $\mathbf{C}$ with the largest eigenvalue λ_m. The in-plane moments are given by the real and imaginary parts of $\boldsymbol{v}_m$. Note that this mode is unique up to a global U(1) rotation which is related to the arbitrary phase of $\boldsymbol{v}_m$.

moment in the thermodynamic limit, where the spins reach approximately 80% of their full moment as $D/J\to\infty$.[39] For all values $D/J>0.1$, it is clear that the finite-size corrections scale as $1/\sqrt{N}$, as expected for a state of broken U(1) symmetry.[40] This scaling procedure represents the appropriate means of deducing the existence of long-ranged magnetic order, by continuing the curves of Fig. 5 to the infinite-system limit. However, this powerful method shows no indication of such order in the regime $0.06\lesssim D/J\lesssim 0.1$, specifying that the transition to the semiclassical state should be taken as $D/J\simeq 0.1$.

The magnetization profile corresponding to the dominant eigenmode $\boldsymbol{v}_m$ also contains important information, which is shown in Fig. 7 for the four representative values of D/J and represented by two-dimensional arrows whose components are the real and imaginary parts of $\boldsymbol{v}_m$. At $D/J\lesssim 0.06$, there is no dominant mode as is the case at large D, but the strongest mode shown in Fig. 7(a) corresponds nevertheless to the pattern of strong spin correlations around the impurity [Fig. 2(a)]: the correlations in this mode are confined to the strong bonds next to the impurity, where the spins are almost antiparallel. The strength of these local correlations is governed by J, which is the reason why λ_m remains essentially D independent, for $D/J\lesssim 0.06$ in Fig. 5. We emphasize again that the profile shown in Fig. 7(a) does not represent the actual magnetization response—this is shown in Fig. 2(a)—but rather the dominant fluctuation mode.

The situation changes dramatically at $D/J\gtrsim 0.1$ [Figs. 7(c) and 7(d)], where the system develops long-ranged order with the majority of spins participating in the $Q=0$ semiclassical 120° state. The data show clearly that the crossover from the dimerlike regime at small D/J to the ordered phase

at high D/J is smooth, and there are no indications for any other type of magnetic order in the intermediate regime $0.06 \lesssim D/J \lesssim 0.1$. This suggests once again that the peculiar magnetization pattern found in Fig. 2(b) is most likely to be a fluctuation effect which is emphasized close to the critical point.

Indeed, our analysis of the magnetic correlations allows us to develop a qualitative understanding of the situation in this regime. The kagome AFM is characterized by a very high density of nearly degenerate states in the ground manifold. The effect of a DM interaction term D is to favor certain states and penalize others, but this process is extremely sensitive to the shape and size of the cluster used in the calculations. Some of our results, such as the discrepancy between Figs. 2(c) and 7(c), are evidence of significant finite-size effects. These effects are expected to, and indeed in Figs. 5 and 6 observed to, increase on approaching the critical regime around $D/J \sim 0.1$. With such small separations between sets of energy levels, the effect of a magnetic field applied in this regime can be dramatic: certainly some of the differences between Figs. 2 and 7 may be ascribed to the finite field in the former. While it remains impossible to exclude more exotic types of order for $0.06 \lesssim D/J \lesssim 0.1$, whose fingerprints might be difficult or even impossible to discern in data obtained from the cluster sizes accessible by exact diagonalization, these considerations make systematic our statement that the most probable explanation for the tendency of the small-D/J and large-D/J data to suggest the presence of an intermediate regime remains in the realm of finite-size effects.

The magnetic correlation data also quantify the extent to which the four sites closest to the impurity continue to resist the effect of D (Fig. 7). As already inferred from the behavior of the correlation amplitudes (Fig. 2), these spins do not adopt a relative 120° orientation, but remain almost antiparallel to each other up to DM interactions $D \sim J$. This direct consequence of frustration relief in the two doped triangles also suggests that the actual orientation of the ordered component of these spins will continue to reflect the behavior of a dimer, and thus will be dictated by **D** and **B** as well as by the coupling to the other spins. Only at surprisingly high values of D/J does a crossover occur to predominant correlation with the other spins of the system, and hence to participation in the 120° ordered state.

This special response of the four sites closest to the impurity is demonstrated once again in Fig. 8, which shows the orientation and magnitude of the spin components obtained from the dominant eigenmode $\boldsymbol{v}_m$. Here the spin magnitude at site i is represented by $\sqrt{\lambda_m}|\boldsymbol{v}_m(i)|$, while the corresponding angle is determined from the phase representation of the real and imaginary parts of $\boldsymbol{v}_m(i)$. The primary feature of Fig. 8 is that, while both the magnitude and the orientation for the majority of sites (open symbols) largely merge together at $D/J \gtrsim 0.06$, the same quantities for the four sites closest to the impurity (filled symbols) remain different up to $D \sim J$. This feature, present in all three clusters, reinforces the picture of the special behavior of the frustration-relieved spins.

V. SUMMARY AND DISCUSSION

We have presented an extensive exact-diagonalization study of the combined effects of nonmagnetic impurities and

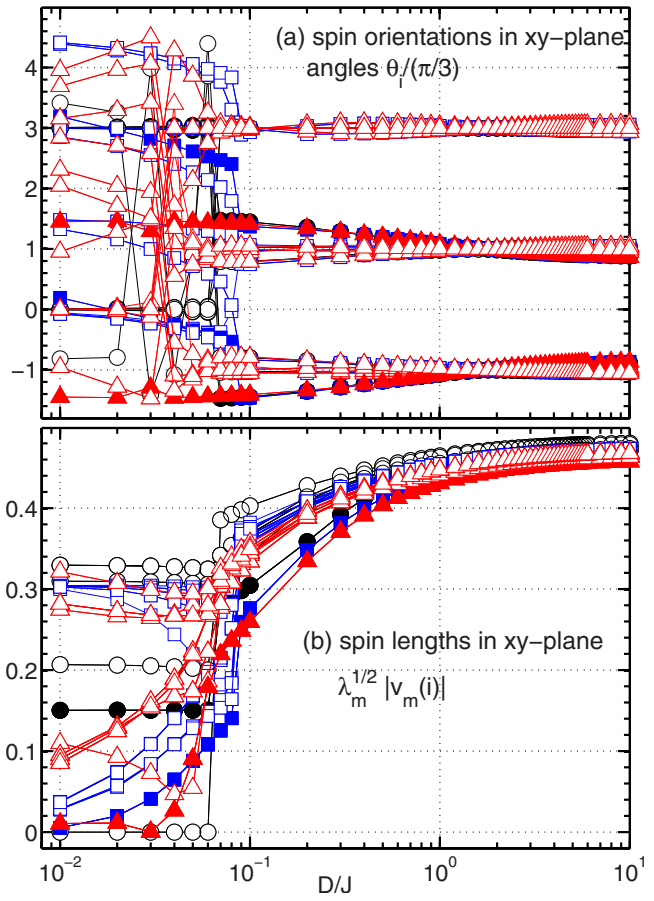

FIG. 8. (Color online) In-plane spin magnitudes and orientations [represented respectively by $\sqrt{\lambda_m}|\boldsymbol{v}_m(i)|$ and by the phase θ_i of $\boldsymbol{v}_m(i)$] as a function of D/J, for clusters with $N=14$ (circles), 20 (squares), and 26 (triangles). The data corresponding to the four sites closest to the impurity are highlighted by filled symbols.

Dzyaloshinskii-Moriya (DM) interactions in the $s=1/2$ kagome antiferromagnet (AFM). Although the clean and purely Heisenberg kagome AFM remains an enigma, being apparently nonmagnetic and possibly dimer based, we have shown how DM interactions immediately induce a magnetic response, and impurities immediately nucleate very strong and somewhat extended patterns of dimerization. We have found that the system undergoes a phase transition from this magnetically disordered state to the $Q=0$ three-sublattice (120°) ordered state when the interaction ratio between the DM and AFM terms is $D/J \sim 0.1$. This conclusion is in agreement with the results obtained by Cépas *et al.* for the clean kagome lattice.[29]

For $D/J \lesssim 0.06$, there is strong dimerization of the spins next to each impurity site as a consequence of frustration relief in these two triangles, as shown by Dommange *et al.*[11] for the $D=0$ case. An oscillating pattern of weakly and strongly dimerized bonds then extends some distance from the impurity site. In the presence of DM interactions, the applied field induces a magnetic response on top of this dimerization pattern, which on the strongly dimerized bonds shows the same qualitative behavior as an isolated dimer, namely, a dominant staggered component directed along $\mathbf{D} \times \mathbf{B}$. The induced magnetic moments on the sites closest to

the vacancy are small as a result of their strong dimerization, and we have shown why the magnetization on the next-nearest strong bonds is approximately four times larger than this. The maximum induced magnetization is thought to occur on these sites or on the next (i.e., next-next-nearest) "ring" of more strongly dimerized bonds beyond them.[11] Still further from the impurity, the local moment decreases again, toward the weak and uniform response (by which is meant no staggered component) of the clean kagome system with DM interactions. Because this is proportional to $\mathbf{D}\times(\mathbf{D}\times\mathbf{B})$, it is much smaller than the staggered response around the impurity sites.

The ordered phase established at $D/J \gtrsim 0.1$ shows all the hallmarks expected for semiclassical magnetic order. However, we found that the spins closest to the impurity remain strongly correlated with each other up to surprisingly large values, $D \sim J$, before they begin to participate fully in the ordered state. Thus a substantial portion of the actual magnetization of these spins remains similar to that of a dimer, and is set by **D** and **B**. Despite the fact that the obvious features of these two phases end at separate values of D/J which leave open the possibility of an intermediate phase, between these limits we have been unable to find any definite evidence for another type of physical behavior. Thus we are forced to the tentative conclusion that there is only one true phase transition in the system, and the features we have observed for $0.06 < D/J < 0.1$ are most likely to be artifacts resulting from the low effective energy scales in this regime and from the small system sizes to which our calculations are constrained.

We conclude by discussing the implications of our results for the interpretation of experiments performed on $ZnCu_3(OH)_6Cl_2$. The most accurate probe of the local magnetic response around doped impurities is NMR, and so we focus on the ^{17}O NMR measurements of Olariu *et al.*[18] Before comparing the experimental results to our calculations, which were performed for a single vacancy in small kagome clusters, it is necessary to consider the impurity concentrations in the experimental samples. Because these are on the order of 5% for the cleaner samples used in the measurements made to date,[18] the average linear spacing between impurities is then 4–5 Cu-Cu bond spacings: in fact this is rather similar to the length scales probed in our $N=20$ and 26 clusters. From our results, it is safe to say that there are no Cu spins in the real material which can be considered as being far from any impurity sites.

Our conclusions show that the situation $D/J > 0.1$ may be safely excluded for herbertsmithite because a magnetically ordered phase of any type is inconsistent not only with the NMR experiments but also with muon spectroscopy and inelastic neutron-scattering experiments,[16,17] where no such order has been found for any temperatures down to 50 mK. By contrast, for DM interactions $D/J < 0.1$, one would expect to observe a broad NMR signal as a consequence of the considerable number of inequivalent Cu sites produced by the partially frozen patterns of dimerization and induced local moments around the randomly distributed impurities. This is compatible with the shape of the M line measured in Ref. 18, while the D line, which probes only one type of Cu site, would indeed be expected to be sharp. Further, our calculations quantify the way in which the DM interaction removes the apparent singlet nature of the $D=0$ ground state, leading to the finite line shift observed in experiment in the limit $T \to 0$.

To be more specific about the actual strength of D/J in herbertsmithite within the disordered regime, we appeal to our results (Sec. III) for the relative local moments on the sites around an impurity. On the qualitative assumption that the ^{17}O line shift should scale with the sum of the moments on the two neighboring Cu sites, the 1:4 moment ratio found for the nearest two Cu sites in the low-D regime ($D/J \lesssim 0.06$) would be expected to result in a 1:5 ratio of the corresponding line shifts. Thus the observed 1:2 ratio[18] suggests quite strongly that herbertsmithite falls in the regime $0.06 \lesssim D/J \lesssim 0.1$. While the exact nature of the ground state in this region remains to be confirmed, it is clear that it is nonmagnetic, and that the moment ratio between the two types of Cu sites closest to an impurity is significantly smaller than at low D/J [Fig. 8(b)]. Such a value for D/J is fully consistent with the result $D \simeq 0.08J$ obtained by electron-spin resonance in Ref. 24.

Finally, we have shown in the disordered regime ($D/J \lesssim 0.1$) that sites close to the impurities exhibit strong features characteristic of the response of isolated dimers, with those right next to an impurity (the D line) reflecting a very weak induced magnetization. This behavior could explain the suppressed local susceptibility at $T \to 0$ and the enhanced nuclear spin-lattice relaxation times T_1 found[18] for these sites. However, to go beyond this qualitative level of agreement, it seems necessary to have access to single-crystal data, which would provide a detailed understanding of the hyperfine interactions in $ZnCu_3(OH)_6Cl_2$. These are required to investigate the dependence of the magnetic response on the field orientation and the line-shift contributions from each Cu site as a function of its induced magnetization, information which could be interpreted directly within our calculational approach.

ACKNOWLEDGMENTS

We are grateful to O. Cépas, C. Lhuillier, P. Mendels, and A. Olariu for fruitful discussions. This work was supported by the Swiss National Science Foundation and by MaNEP.

APPENDIX A: LINEAR RESPONSE OF THE FOUR-SITE CLUSTER

Here we present the details of the magnetic response of the four-site cluster shown in Fig. 9, and demonstrate why this can be considered as the minimal cluster illustrating the physics of the low-D regime. The Hamiltonian is

$$\mathcal{H} = \mathcal{H}_1 + \mathcal{H}_2 + \mathcal{V} \equiv \mathcal{H}_0 + \mathcal{V}, \tag{A1}$$

in which

$$\mathcal{H}_1 = J(\mathbf{s}_1 \cdot \mathbf{s}_2 + \mathbf{s}_3 \cdot \mathbf{s}_4) - \mathbf{B} \cdot \mathbf{S}, \tag{A2}$$

$$\mathcal{H}_2 = J(\mathbf{s}_2 \cdot \mathbf{s}_3 + \mathbf{s}_2 \cdot \mathbf{s}_4), \tag{A3}$$

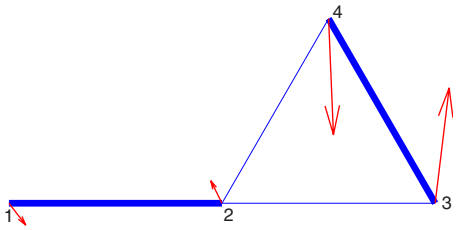

FIG. 9. (Color online) Typical in-plane magnetization pattern (red arrows) and spin correlation functions (represented in blue by the bond thickness) for the minimal four-site cluster in the small-D regime. Here $D=B=J/20$, $\theta=30°$, and the orientations of the DM interactions are the same as for sites 1–4 in Fig. 1.

$$\mathcal{V}=\mathbf{D}\cdot(\mathbf{s}_2\times\mathbf{s}_1+\mathbf{s}_2\times\mathbf{s}_3+\mathbf{s}_3\times\mathbf{s}_4+\mathbf{s}_4\times\mathbf{s}_2), \quad \text{(A4)}$$

$\mathbf{S}=\Sigma_i\mathbf{s}_i$ is the total spin, $\mathbf{D}=D\mathbf{e}_z$, and $\mathbf{B}$ lies in the xz plane, as shown in Fig. 1. Our purpose is to examine the magnetization response of this cluster for small fields and to explain why this captures the generic response of the corresponding sites around the impurity in Fig. 2. We find numerically that to leading order in D/J there is a staggered response along the y axis given by

$$\langle\mathbf{s}_1\rangle=-\langle\mathbf{s}_2\rangle=\frac{1}{2}\mathbf{D}\times\mathbf{B}, \quad \text{(A5)}$$

$$\langle\mathbf{s}_3\rangle=-\langle\mathbf{s}_4\rangle=\frac{21}{8}\mathbf{D}\times\mathbf{B}, \quad \text{(A6)}$$

i.e., the magnetization response at bond (1,2) is precisely that expected for an isolated dimer while, surprisingly, the response at the bond (3,4) is approximately five times greater. We provide a qualitative interpretation of this result based on the character of the excitations of $\mathcal{H}_0$.

Using $\mathcal{V}$ as a perturbation, the ground state is given to leading order by $|\psi\rangle=(1+\mathcal{R}\mathcal{V})|\psi_0\rangle$, where $|\psi_0\rangle$ is the ground state of $\mathcal{H}_0$, $\mathcal{R}=\frac{Q}{E_0-\mathcal{H}}$ is the corresponding resolvent operator with $Q=1-|\psi_0\rangle\langle\psi_0|$, and $E_0=-3J/2$. The mean value of any operator A is then given by

$$\langle A\rangle=\langle\psi_0|A\mathcal{R}\mathcal{V}|\psi_0\rangle+\text{H.c.}, \quad \text{(A7)}$$

where we have assumed that $\langle\psi_0|A|\psi_0\rangle=0$. Because this relation gives the linear response, it may be used to obtain the individual contribution of any of the DM terms contained in $\mathcal{V}$ to the magnetization of any spin site.

For each of the bonds (1,2) and (3,4), it is convenient to use the singlet and triplet basis states $|s\rangle=(|\uparrow\downarrow\rangle-|\downarrow\uparrow\rangle)/\sqrt{2}$, $|t_1\rangle=|\uparrow\uparrow\rangle$, $|t_0\rangle=(|\uparrow\downarrow\rangle+|\downarrow\uparrow\rangle)/\sqrt{2}$, and $|t_{-1}\rangle=|\downarrow\downarrow\rangle$. For $B<J/2$, the ground state $|\psi_0\rangle$ of $\mathcal{H}_0$ is the product state of the two singlets,

$$|\psi_0\rangle=|s\rangle_{12}\otimes|s\rangle_{34}. \quad \text{(A8)}$$

Also applicable are the relations[41]

$$\mathcal{H}_2|s\rangle_{12}\otimes|s\rangle_{34}=0, \quad \text{(A9)}$$

$$\mathcal{H}_2|t_m\rangle_{12}\otimes|s\rangle_{34}=0, \quad \forall\, m=0,\pm1, \quad \text{(A10)}$$

which specify that the state $|t_m\rangle_{12}\otimes|s\rangle_{34}$ is also an eigenstate of $\mathcal{H}_0$. Thus the local excitation of a triplet on bond (1,2), for example by acting with the term $\mathbf{D}\cdot\mathbf{s}_2\times\mathbf{s}_1$ (or the operators $A=s^y_{1,2}$) on $|\psi_0\rangle$, gives

$$\mathcal{R}|t_m\rangle_{12}\otimes|s\rangle_{34}=\frac{-1}{1+mB}|t_m\rangle_{12}\otimes|s\rangle_{34}, \quad \text{(A11)}$$

and the triplet remains localized.

By contrast, a triplet on bond (3,4) will not remain localized because $|s\rangle_{12}\otimes|t_m\rangle_{34}$ is not an eigenstate of $\mathcal{H}_0$. With these considerations and by using Eq. (A7), it is easy to show that of all the DM terms contained in $\mathcal{V}$, only $\mathbf{D}\cdot\mathbf{s}_2\times\mathbf{s}_1$ contributes to $\langle\mathbf{s}_{1,2}\rangle$, and this explains in turn why the response at bond (1,2) is that of an isolated dimer. The staggered magnetization at bond (3,4), on the other hand, is driven by all the terms of $\mathcal{V}$ except $\mathbf{D}\cdot\mathbf{s}_2\times\mathbf{s}_1$, which explains why this is different from the response of bond (1,2). More generally, we see that although the ground state of $\mathcal{H}_0$ is a product of two dimers, the different character of the local excitations leads to quantitatively very different responses. This completes the qualitative interpretation, summarized in Sec. III, for the different magnetization responses of the sites around the impurity in Fig. 2.

APPENDIX B: INTERPRETATION OF MAGNETIC CORRELATIONS

Here we provide a more detailed presentation of the natural orbital method used in Sec. IV for the study of in-plane magnetic correlations. We consider the ground state $|\Psi\rangle$ of the Hamiltonian given in Eq. (1) and express the in-plane magnetic correlations by the matrix $\mathbf{C}$ of Eq. (4). Let us denote by $\{\lambda_a,\boldsymbol{v}_a\}$ the set of eigenvalues and normalized eigenvectors of $\mathbf{C}$, i.e., $\mathbf{C}\cdot\boldsymbol{v}_a=\lambda_a\boldsymbol{v}_a$. In addition to being Hermitian, the correlation matrix $\mathbf{C}$ is also positive semidefinite because for any normalized vector $\boldsymbol{v}$ one has $\boldsymbol{v}^\dagger\cdot\mathbf{C}\cdot\boldsymbol{v}=\|\mathcal{M}_{\boldsymbol{v}}|\Psi\rangle\|^2\geq0$, where

$$\mathcal{M}_{\boldsymbol{v}}\equiv\sum_i\boldsymbol{v}(i)s_i^- \quad \text{(B1)}$$

defines a macroscopic magnetic mode. Thus $\lambda_a\geq0$ for all a. Further, because $s^+s^-=1/2+s^z$ for $s=1/2$, $\text{Tr}\,\mathbf{C}=\Sigma_a\lambda_a=N/2+\langle S^z\rangle$. We note also that the eigenvalues λ_a give the fluctuations of the matrix $\mathcal{M}_a$ [specified by Eq. (B1) with $\boldsymbol{v}=\boldsymbol{v}_a$] because

$$\langle\Psi|\mathcal{M}_a^\dagger\mathcal{M}_b|\Psi\rangle=\lambda_a\delta_{ab}. \quad \text{(B2)}$$

In order to discuss magnetic order, we consider the thermodynamic limit and address the question of what is required to ensure long-ranged in-plane magnetic correlations, i.e.,

$$\lim_{|i-j|\to\infty}C_{ij}\neq0. \quad \text{(B3)}$$

To this end, it is convenient to express $\mathbf{C}$ in terms of its spectral decomposition,

$$C_{ij} = \sum_a \lambda_a \boldsymbol{v}_a(i)\boldsymbol{v}_a^*(j). \tag{B4}$$

Equations (B3) and (B4) mean that there should exist at least one eigenstate $\boldsymbol{v}_m$ with a nonzero amplitude $\boldsymbol{v}_m(i)$ for all i. However, $\boldsymbol{v}$ is a quantity normalized to one by an overall factor of $1/\sqrt{N}$, which from Eq. (B3) means that the corresponding eigenvalue is macroscopically large, $\lambda_m \propto N$. If only one (the maximum) eigenvalue has this property, it is safe to replace Eq. (B4) with

$$C_{ij} \simeq \lambda_m \boldsymbol{v}_m(i)\boldsymbol{v}_m^*(j) \tag{B5}$$

because the neglected terms are negligibly small for $N \to \infty$. This special separable form of the correlation matrix in an ordered state allows one to identify the relevant local order parameter. Indeed, in an explicitly symmetry-broken (coherent) state we may replace $\langle s_i^+ s_j^- \rangle$ by $\langle s_i^+ \rangle \langle s_j^- \rangle$, and hence make the identification

$$\langle s_i^+ \rangle = \langle s_i^x \rangle + i\langle s_i^y \rangle = \sqrt{\lambda_m}\boldsymbol{v}_m(i). \tag{B6}$$

We remark here that these in-plane spin components are fixed only up to a global U(1) rotation due to the fact that the eigenstate $\boldsymbol{v}_m$ is only specified up to a global phase. The corresponding macroscopic order parameter is given by $\mathcal{M}_m$ because [using Eq. (B2)]

$$\langle \Psi | \mathcal{M}_m^\dagger \mathcal{M}_m | \Psi \rangle = \lambda_m \propto N, \tag{B7}$$

and thus the response to a conjugate field that couples directly to $\mathcal{M}_m$ diverges in the thermodynamic limit.

Finally we should mention the analogy of the discussion presented in this appendix to Bose-Einstein condensation, and in particular to the case of cold-atom systems confined in a harmonic trap (see for example Ref. 42). The correlation matrix in such a system is the one-body density matrix, $\rho_1(\mathbf{x},\mathbf{x}')$, which measures the coherence between different parts of the system. The eigenstates of ρ_1 are termed "the natural orbitals", and the eigenvalues give the relative occupation probability of these orbitals. As in our situation, off-diagonal long-range order is signaled by the fact that one of the eigenvalues of ρ_1 becomes macroscopically large.[37,38] The dominant eigenstate $\boldsymbol{v}_m$ of a magnetic system is thus analogous to the condensate wave function in a superfluid.

[1] G. Misguich and C. Lhuillier, in *Frustrated Spin Systems*, edited by H. T. Diep (World Scientific, Singapore, 2005).
[2] P. W. Anderson, Mater. Res. Bull. **8**, 153 (1973).
[3] J. B. Marston and C. Zeng, J. Appl. Phys. **69**, 5962 (1991); A. V. Syromyatnikov and S. V. Maleyev, Phys. Rev. B **66**, 132408 (2002); P. Nikolic and T. Senthil, *ibid.* **68**, 214415 (2003); R. Budnik and A. Auerbach, Phys. Rev. Lett. **93**, 187205 (2004); R. R. P. Singh and D. A. Huse, Phys. Rev. B **76**, 180407(R) (2007).
[4] S. Sachdev, Phys. Rev. B **45**, 12377 (1992); F. Wang and A. Vishwanath, *ibid.* **74**, 174423 (2006).
[5] F. Mila, Phys. Rev. Lett. **81**, 2356 (1998).
[6] H. C. Jiang, Z. Y. Weng, and D. N. Sheng, Phys. Rev. Lett. **101**, 117203 (2008).
[7] M. B. Hastings, Phys. Rev. B **63**, 014413 (2000).
[8] Y. Ran, M. Hermele, P. A. Lee, and X.-G. Wen, Phys. Rev. Lett. **98**, 117205 (2007); M. Hermele, Y. Ran, P. A. Lee, and X.-G. Wen, Phys. Rev. B **77**, 224413 (2008).
[9] M. Elhajal, B. Canals, and C. Lacroix, Phys. Rev. B **66**, 014422 (2002).
[10] R. Ballou, B. Canals, M. Elhajal, C. Lacroix, and A. S. Wills, J. Magn. Magn. Mater. **262**, 465 (2003).
[11] S. Dommange, M. Mambrini, B. Normand, and F. Mila, Phys. Rev. B **68**, 224416 (2003).
[12] A. Läuchli, S. Dommange, B. Normand, and F. Mila, Phys. Rev. B **76**, 144413 (2007).
[13] M. P. Shores, E. A. Nytko, B. M. Barlett, and D. G. Nocera, J. Am. Chem. Soc. **127**, 13462 (2005).
[14] M. Rigol and R. R. P. Singh, Phys. Rev. Lett. **98**, 207204 (2007).
[15] G. Misguich and P. Sindzingre, Eur. Phys. J. B **59**, 305 (2007).
[16] P. Mendels, F. Bert, M. A. de Vries, A. Olariu, A. Harrison, F. Duc, J.-C. Trombe, J. S. Lord, A. Amato, and C. Baines, Phys. Rev. Lett. **98**, 077204 (2007).
[17] J. S. Helton, K. Matan, M. P. Shores, E. A. Nytko, B. M. Bartlett, Y. Yoshida, Y. Takano, A. Suslov, Y. Qiu, J.-H. Chung, D. G. Nocera, and Y. S. Lee, Phys. Rev. Lett. **98**, 107204 (2007).
[18] A. Olariu, P. Mendels, F. Bert, F. Duc, J. C. Trombe, M. A. de Vries, and A. Harrison, Phys. Rev. Lett. **100**, 087202 (2008).
[19] S.-H. Lee, H. Kikuchi, Y. Qiu, B. Lake, Q. Huang, K. Habicht, and K. Kiefer, Nat. Mater. **6**, 853 (2007).
[20] M. A. de Vries, K. V. Kamenev, W. A. Kockelmann, J. Sanchez-Benitez, and A. Harrison, Phys. Rev. Lett. **100**, 157205 (2008).
[21] F. Bert, S. Nakamae, F. Ladieu, D. L'Hôte, P. Bonville, F. Duc, J.-C. Trombe, and P. Mendels, Phys. Rev. B **76**, 132411 (2007).
[22] M. Mambrini and F. Mila, Eur. Phys. J. B **17**, 651 (2000).
[23] I. Dzyaloshinsky, J. Phys. Chem. Solids **4**, 241 (1958); T. Moriya, Phys. Rev. Lett. **4**, 228 (1960).
[24] A. Zorko, S. Nellutla, J. van Tol, L. C. Brunel, F. Bert, F. Duc, J.-C. Trombe, M. A. de Vries, A. Harrison, and P. Mendels, Phys. Rev. Lett. **101**, 026405 (2008).
[25] R. Moessner, Can. J. Phys. **79**, 1283 (2001).
[26] A. B. Harris, C. Kallin, and A. J. Berlinsky, Phys. Rev. B **45**, 2899 (1992).
[27] A. Chubukov, Phys. Rev. Lett. **69**, 832 (1992).
[28] C. L. Henley and E. P. Chan, J. Magn. Magn. Mater. **140-144**, 1693 (1995).
[29] O. Cépas, C. M. Fong, P. W. Leung, and C. Lhuillier, Phys. Rev. B **78**, 140405(R) (2008).
[30] M. Tovar, K. S. Raman, and K. Shtengel, Phys. Rev. B **79**, 024405 (2009).
[31] K. Gregor and O. I. Motrunich, Phys. Rev. B **77**, 184423 (2008).
[32] M. J. Rozenberg and R. Chitra, Phys. Rev. B **78**, 132406 (2008).
[33] Y. F. Cheng, O. Cépas, P. W. Leung, and T. Ziman, Phys. Rev. B **75**, 144422 (2007).
[34] D. Poilblanc, A. Läuchli, M. Mambrini, and F. Mila, Phys. Rev. B **73**, 100403(R) (2006).

[35] S. Miyahara, J.-B. Fouet, S. R. Manmana, R. M. Noack, H. Mayaffre, I. Sheikin, C. Berthier, and F. Mila, Phys. Rev. B **75**, 184402 (2007).
[36] S. Capponi, A. Läuchli, and M. Mambrini, Phys. Rev. B **70**, 104424 (2004).
[37] O. Penrose and L. Onsager, Phys. Rev. **104**, 576 (1956).
[38] C. N. Yang, Rev. Mod. Phys. **34**, 694 (1962).
[39] We note here that the extrapolated values of the (unrescaled) squared moments reported for the clean kagome system in Ref. 29 are smaller than the true values by a factor of two. The origin of this factor lies in the choice of the x components of the spins for studying the correlations: the dominant eigenvalue of these correlations is twofold degenerate and corresponds to two modes with the same magnetization pattern in the x direction but with different chirality. By contrast, the correlation matrix **C** defined in Eq. (4) is able to select the state with the correct chirality, namely, that favored by the DM interactions.
[40] H. Neuberger and T. Ziman, Phys. Rev. B **39**, 2608 (1989); D. S. Fisher, *ibid.* **39**, 11783 (1989).
[41] S. Miyahara and K. Ueda, Phys. Rev. Lett. **82**, 3701 (1999).
[42] J. L. DuBois and H. R. Glyde, Phys. Rev. A **63**, 023602 (2001).